603 050

SSD-TDR-64-124

Report No.
TDR-269(4240-10)-14

29 p $2.00 hc
$0.50 mf

MICROPLASTICITY

Prepared by

R. D. Carnahan
Materials Sciences Laboratory

Laboratory Operations
AEROSPACE CORPORATION
El Segundo, California

Contract No. AF 04(695)-269

15 July 1964

Prepared for

BALLISTIC SYSTEMS AND SPACE SYSTEMS DIVISIONS
AIR FORCE SYSTEMS COMMAND
LOS ANGELES AIR FORCE STATION
Los Angeles, California

SSD-TDR-64-124

Report No.
TDR-269(4240-10)-14

MICROPLASTICITY

Prepared

R. D. Carnahan

Approved

W. C. Riley, Head
Applied Science Department

J. E. Hove, Director
Materials Sciences Laboratory

This technical documentary report has been reviewed and is approved for publication and dissemination. The conclusions and findings contained herein do not necessarily represent an official Air Force position.

For Space Systems Division
Air Force Systems Command

Werner J. Iller
Major, USAF

ABSTRACT

This report presents a review of experimental methods for measuring plastic deformation that occurs at strains of $\sim 1 \times 10^{-6}$ in./in. plastic Dislocation theory is applied to predict microstrain values for selected engineering materials, and calculated and experimental results are compared. It is demonstrated that a simplified theoretical approach can be used to predict the microstrain behavior to be expected for typical engineering materials.

CONTENTS

TABLES

FIGURES

I. INTRODUCTION

A microstrain is defined as a strain of 1×10^{-6} in./in., and in this report, all plastic deformation that occurs at strains below about 1×10^{-4} in./in. plastic will be referred to as microplastic deformation. Historically, the cognizance of a region of microplastic flow can be traced to the development of research techniques to the point where resolution of permanent microstrains of this magnitude became measurable. One of the earliest experimental reports of a microstrain observation was in 1925, when Haase and Schmid,[1] studying the plasticity limit of zinc, determined that it showed a plastic strain of $\sim 1 \times 10^{-5}$ in./in. at a stress of one-half the macroscopic yield stress. We know now, of course, that this represents only the lower limit of the measuring sensitivity at that time, which was $\sim 1 \times 10^{-5}$. To illustrate the region of interest, Figure 1 shows a typical stress-strain curve, with the apparent elastic region enlarged to show the relative region of microstrain.

Although it was recognized that microscopic pre-yield plastic strain occurred, there was very little interest in microstrain studies until late in the 1940's when experimental efforts designed to verify dislocation theory were reported. Determination of non-elastic behavior and departures from linear elastic behavior was of definite interest for the development of dislocation theory with its basis in elasticity theory; hence, it became pertinent to study the early stages of deformation, i.e., the microstrain region. Much of the early work on delay-yielding behavior and microstrain of low carbon steels was carried out at Cal Tech by Wood and Clark[2] and associates[3, 4] in an effort to relate mechanical behavior to the dynamical behavior of dislocations. Since the mid 1950's, Brown of the University of Pennsylvania has been actively engaged in microstrain research and with his associates has contributed substantially to the development of techniques for these studies.[5-8]

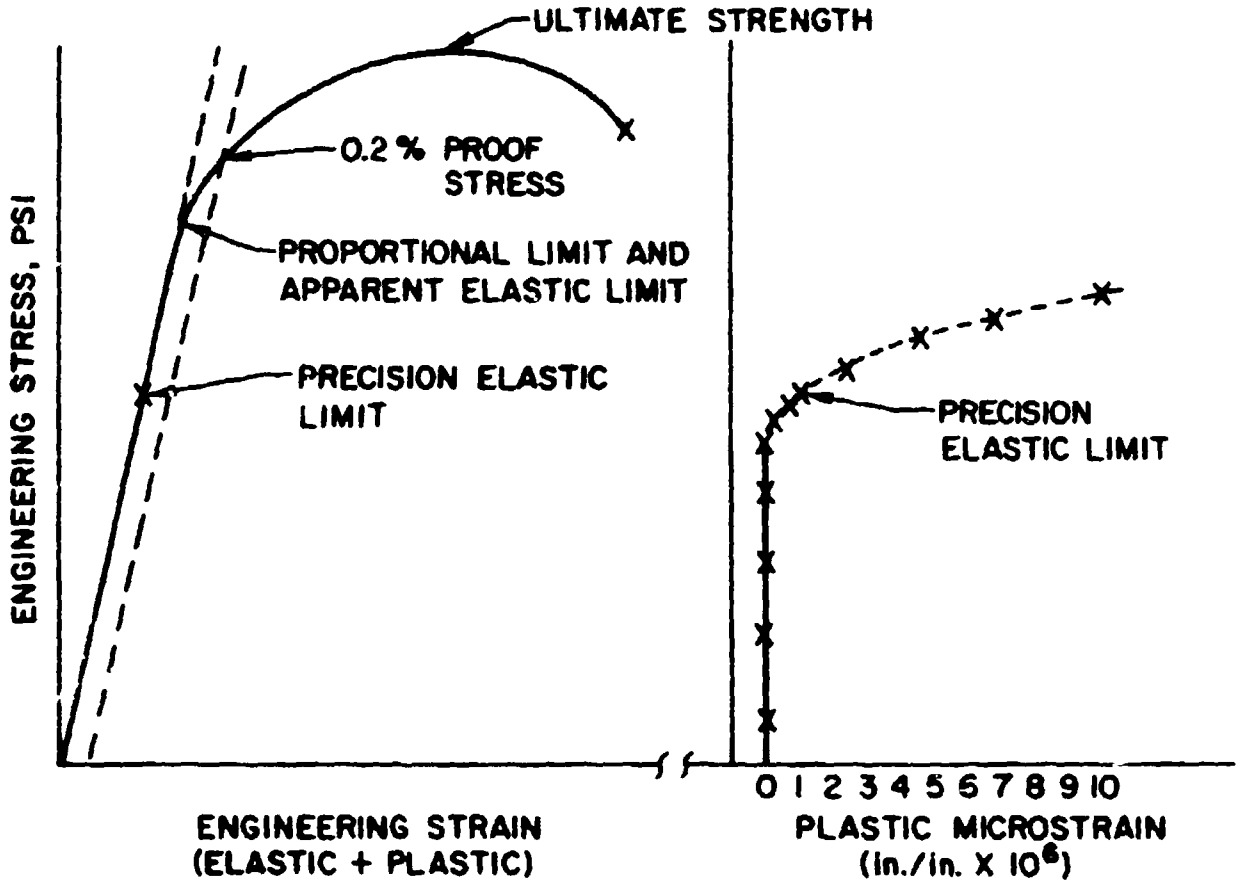

Figure 1. A Typical Stress-Strain Curve

The steadily increasing interest in the field is further emphasized by the fact that a symposium on microstrain was held in conjunction with the annual meeting of the Institute of Metals Division of the A. I. M. E. in New York in February 1964, and a group of 20 papers was presented on the subject. The breadth of the field is implied by the fact that dynamic internal friction studies relating to amplitude dependent damping losses (dislocation damping) were grouped with more traditional quasi-dynamic studies of microstrain.

Recently, interest in this region of strains has also developed for other than purely scientific reasons. The materials engineer is now confronted with the need to specify completely and precisely the mechanical behavior of materials for use in space systems (e.g., control and guidance systems components) where dimensional stability is required in both static and dynamic mechanical environments. The importance of this problem is illustrated in the following tables. Table 1 lists the relative guidance requirements needed for various missile systems and possible missions. Table 2 shows the gyro drift rate errors that can be produced by potential gyro rotor shifts for two hypothetical gyros, each operating under two dynamic conditions. (Note that for the reference system to detect a gyro drift rate error of 0.01 deg/hr the gyro reference platform must be stable to ~2 sec of arc, i.e., have a dimensional stability of ~10 μin./in.)

To see how materials limitations might affect accuracy level, consider the hypothetical ICBM discussed by G Harter.[9] If it is assumed that the gyro reference platform undergoes a dimensional change of 0.1 arc-sec/g of acceleration and that the gyro rotor experiences a center of gravity shift of 1 μin./in., the corresponding velocity errors produced by these changes are sufficient to cause the hypothetical missile to fall 1000 ft short of its target during a 300-sec flight time. In other words ten percent of the permissible error, assuming an ICBM with ±1 mile accuracy represents a current limit in technology, is accounted for by permanent deformations in the microstrain region. For more critical missions, such limitations may be intolerable. Thus, it is clear that the present need for determining micromechanical properties extends well beyond a purely scientific interest.

Table 1. Relative Requirements for Guidance System Accuracies for Military and Space Missions (Ref. 10)

System	Accuracy, mi	Max Velocity Error Per 10^4 ft/sec, ft/sec
V2	± 20	50.0
Scientific Satellite	± 100	80.0
Moon Impact		20.0
ICBM	± 10	5.0
Moon Impact	± 100	1.0
ICBM	± 1	0.5
Mars Impact		0.4
Cislunar Flight		0.3

Table 2. Gyro Error Torques (Ref. 11)

Gyro Angular Momentum, gm-cm^2/sec	Weight, gm	Error Drift Rate, deg/hr	Error Torque Drift Rate, dyne-cm	Equivalent Rotor Shift, in.
1×10^5	35	0.1	0.05	2×10^{-6}
1×10^5	35	0.01	0.005	2×10^{-7}
2×10^6	260	0.01	1.0	4×10^{-6}
2×10^6	260	0.001	0.1	4×10^{-7}

II. TECHNIQUES FOR MEASURING MICROSTRAIN

A number of techniques to measure and study the micro-properties of materials are at the disposal of the materials scientist and engineer in most industrial, governmental, and university laboratories. The means may include optical-mechanical or electronic systems, techniques for measuring internal friction, or etch pitting techniques. Some of the most widely used methods will be discussed in this section.

A. OPTICAL-MECHANICAL SYSTEMS

The best known optical-mechanical system is the Tuckerman optical strain gage shown in Figure 2, which operates on the principle of an optical lever system composed of three mirrors. The strain is measured through an auto-collimator and is detected as a rocking of the lozenge and prism. This system is capable of resolving strains of $\sim \pm 1 \times 10^{-6}$ in./in. Application for this gage has been found in precision elastic limit (P.E.L.) studies, and it is currently used to determine precision micro-properties of beryllium and other materials--both for fundamental understanding and for application to guidance and control systems.[12]

B. ELECTRONIC SYSTEMS

Brown and his co-workers[5-8] use an electronic system that is a capacitance gage adaptation for precision strain measurements in a tensile configuration. This arrangement, shown in Figure 3, is based on the principle of measuring the capacitance of an air gap between two parallel condenser plates. The capacitance C, measured in micromicrofarads, is

$$C = 0.225K\,(A/d) \qquad (1)$$

where K is the dielectric constant of the medium, d the separation of plates in inches, and A the plate area in square inches. A change in displacement Δd produces a change in capacitance ΔC given by

$$\Delta d = \frac{-\Delta C}{0.225KA}\, d^2 \qquad (2)$$

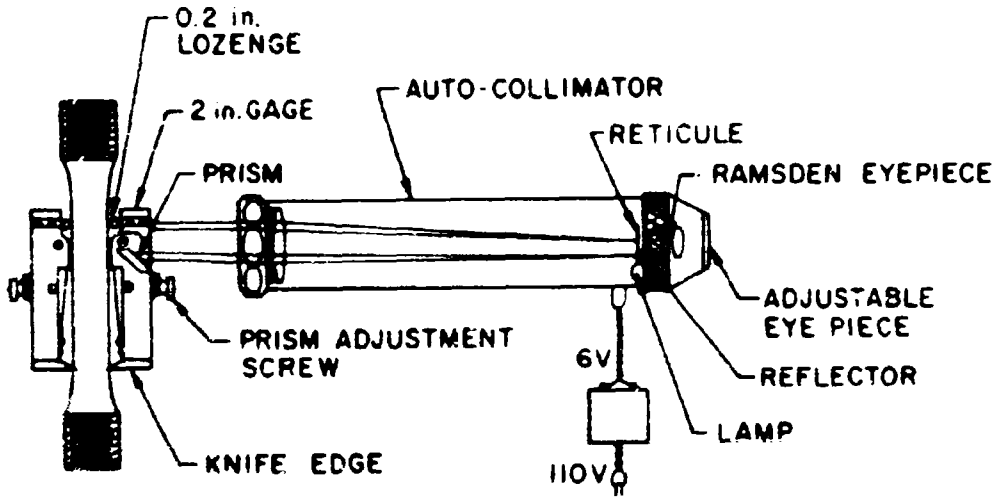

Figure 2. Tuckerman Optical Strain Gage

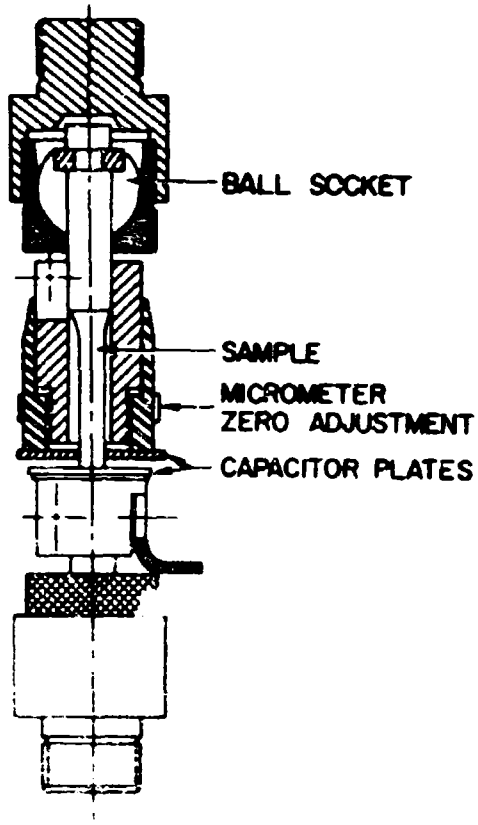

Figure 3. Capacitance Gage Adaptation for Precision Strain Measurements

Depending upon the accuracy with which ΔC is measurable and the magnitudes of A and d, one can ideally measure Δd of 10^{-8} in. For example, using a Fielden proximity meter measuring a ΔC of 0.01 $\mu\mu f$ with A = 1 and d = 0.004, Brown and Roberts[5,7] report a sensitivity of 10^{-8} inches.

The electronic system currently most commonly used for microstrain measurements utilizes convensional foil or wire strain gage technology, where a tensile sample is mounted with strain gages R_1 and R_4 of a conventional bridge circuit as shown in Figure 4. Dummy gages R_2 and R_3 are mounted on a second sample suspended nearby to give temperature compensation. The ratio of the change in resistance $\Delta R/R_{original}$ is proportional to the relative change in length of the gage wires $\Delta L/L$, which is a measure of strain. Hence, the sensitivity attainable is governed by the sensitivity of the measuring potentiometer, the number of gages actively employed, the gage factor, and gage resistivity. Depending on these factors and the noise level of the amplification system, deflections as small as 5×10^{-8} in. can be measured with bonded foil gages. This limit can be extended at least an order of magnitude by using semiconductor strain gages.

Other techniques easily capable of measuring strain sensitivities of $\pm 1 \times 10^{-6}$ in./in. or better can be set up using eddy current proximity gages and linear differential transformers (LDT).

One of the major shortcomings in each of the preceding systems that generally limits sensitivity to $\pm 2 \times 10^{-6}$ in./in. in spite of the ideal sensitivity available is temperature control. Most engineering materials exhibit thermal coefficients of linear expansion of 5×10^{-6} in./in./°C or greater so that unless care is taken to control test temperature and to carefully match the expansion coefficients of the various components of the testing assembly, temperature fluctuations as small as 0.1°C can produce errors of about 1×10^{-6} in./in.

The temperature problems may be countered by careful selection of materials and matching of coefficients, precise temperature control and elimination of localized thermal gradients, and mechanical design in testing

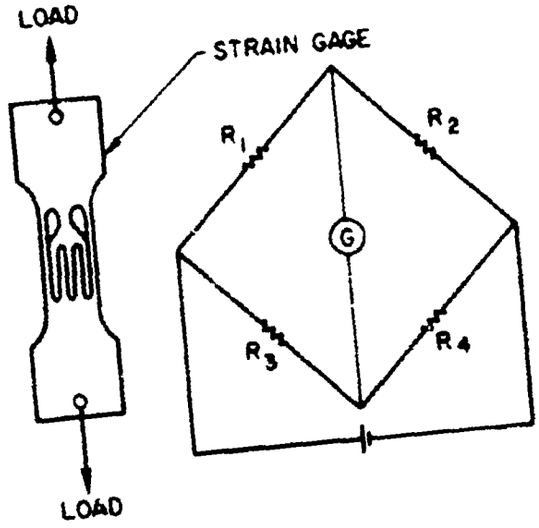

Figure 4. Foil or Wire Strain Gage for Tensile Testing

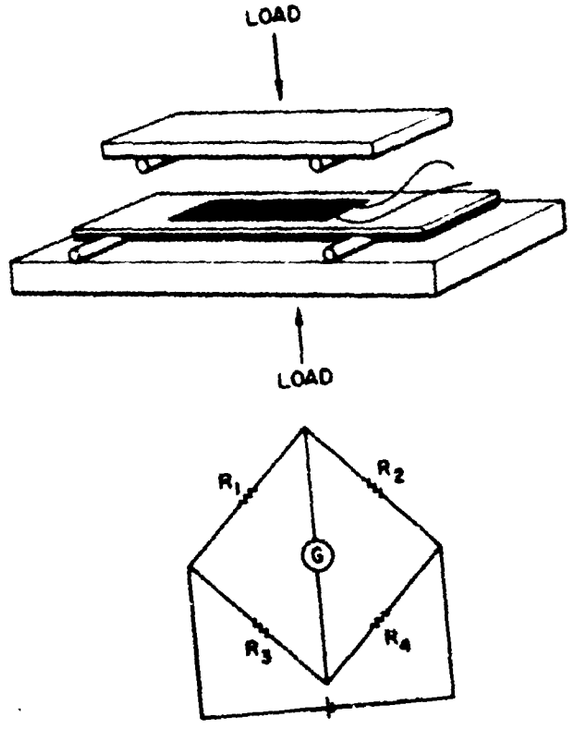

Figure 5. Four-Point Bending Configuration with Strain Gages

to avoid linear expansion differences (e.g., torsion testing which can be done with LDT, capacitance, and proximity gages and a four-point bending technique using foil or wire strain gages.) The test configuration for the four-point bending technique[13] is shown in Figure 5, where gages R_1 and R_2 are mounted in tension and compression, respectively. The signals are additive when the sample is subjected to a bending stress which doubles the strain sensitivity. The generation of an apparent compressive tensile strain such as is imposed by a negative temperature change, however, results in no net signal since the two gages experience like changes that are nulled out in the bridge circuit. Temperature control is therefore eliminated as a variable since only strains produced in bending generate a bridge unbalance.

C. INTERNAL FRICTION MEASURING TECHNIQUES

The study of internal friction has generated a family of techniques for measuring microstrains. These are too numerous to review in detail but in general involve measuring the damping losses associated with a sample vibrating at resonance in either a driven or freely vibrating arrangement. Microstrain is manifested by a dependence of damping capacity on the amplitude of vibration in full cycle loading, e.g., the sample is cycled sinusoidally from positive to negative stress through zero and the loss tangent is determined. Amplitude dependent losses are associated with hysteresis in the response of line imperfections (dislocations) to the oscillating stress. A typical system for measuring low-frequency internal friction[14] is shown in Figure 6; Figure 7 shows a characteristic damping curve obtained using this apparatus.[15] Since the damping factor Q^{-1} is proportional to the ratio of the anelastic to elastic strains, and typical Q^{-1} values are 10^{-5} to 10^{-3}, the anelastic strains are of the order 10^{-11} to 10^{-7} in./in.

D. ETCH PITTING TECHNIQUES

Etch pitting techniques have been used chiefly to study individual dislocation motion, which in the present context would represent heterogeneous strain. The measurements by Gilman and Johnston[16] of the dislocation velocity of LiF constitute the classic use of this approach. Young[17] has also

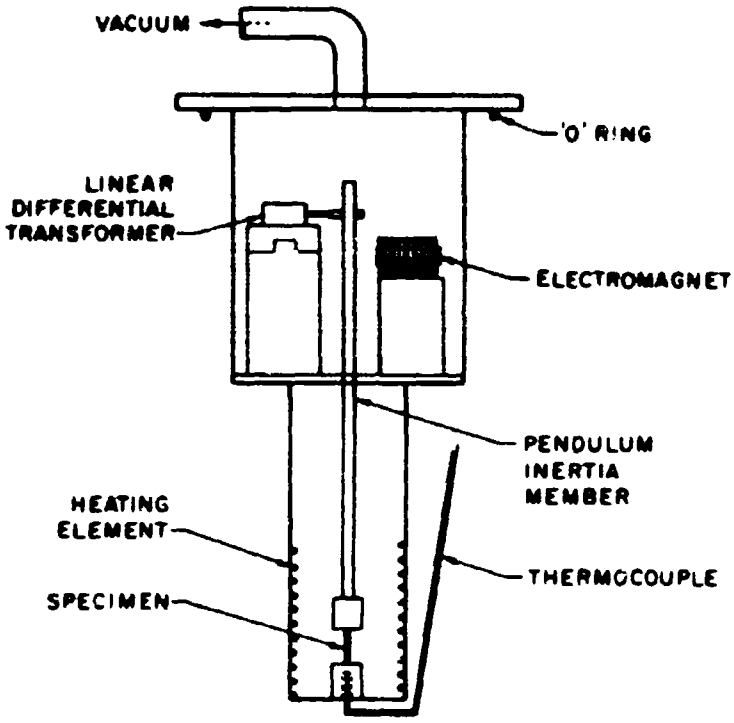

Figure 6. Typical System for Measuring Low-Frequency Internal Friction

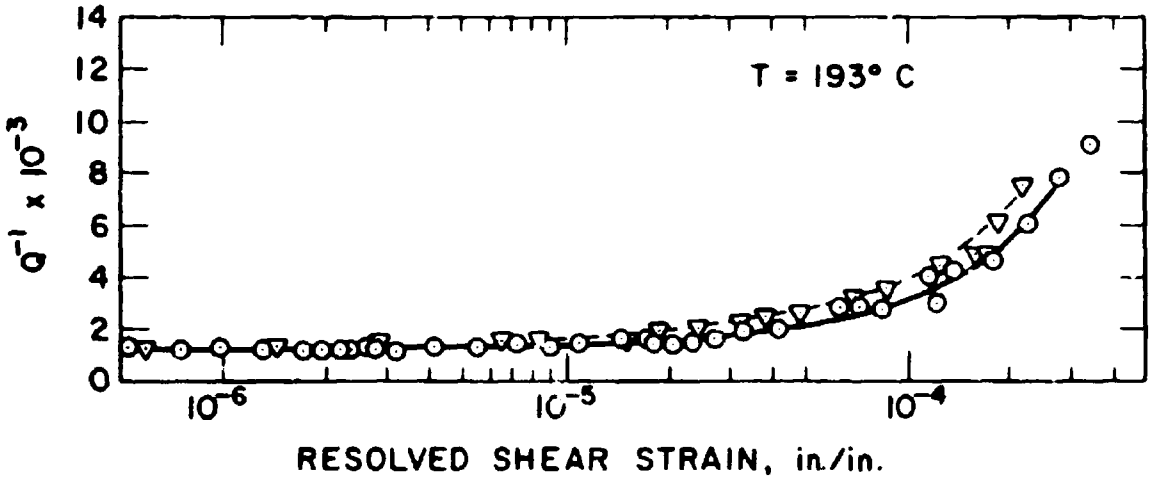

Figure 7. Characteristic Damping Curve Obtained with Internal Friction Measuring Device

used this technique to observe dislocation motion in copper single crystals and has observed irreversible dislocation motion at $\tau = 4$ gm/mm^2 and dislocation multiplication at $\tau \cong 18$ gm/mm^2. In studies on polycrystalline OFHC copper, finite deformation has been observed at a resolved stress of 13 gm/mm^2 using the four-point bending technique.*

The ranges of strains that can be examined with the various techniques discussed in this section are summarized in Figure 8. The most common test is for determination of the P.E.L. The technique for this test is comprised of steps of loading the sample to a finite stress, instantaneously unloading on reaching maximum stress, and measuring the residual plastic strain (see Figure 9). Each successive step is carried out at a higher stress until a permanent strain of 1 or 2×10^{-6} in./in. is attained. Other special purpose tests involve changes in strain rate ranging from dead loading (to observe microscreep) to continuous loading with precise resolution of total strain.

*R.D. Carnahan, Unpublished Data.

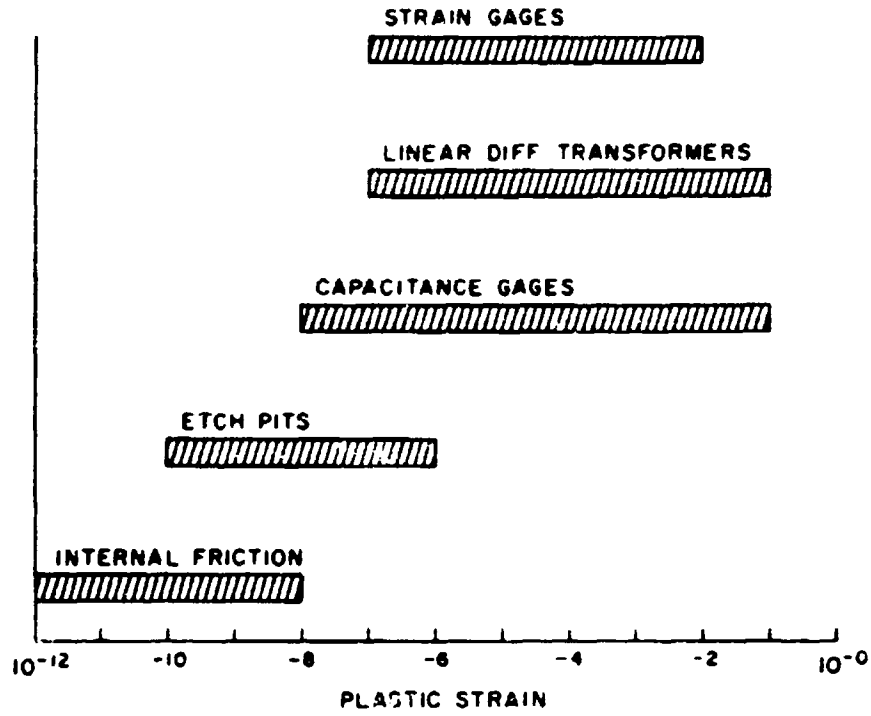

Figure 8. Ranges of Strain Measured by Various Techniques

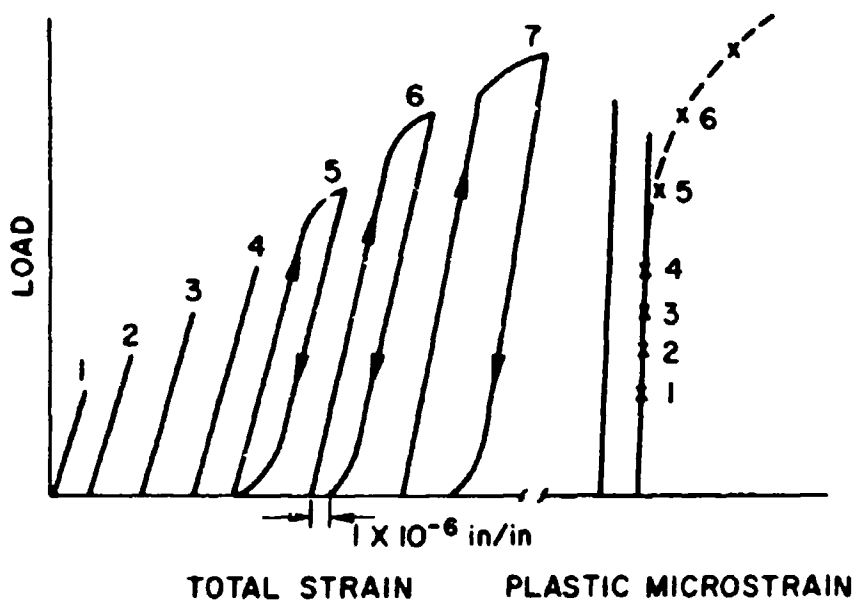

Figure 9. A Typical Precision Elastic Limit (P. E. L.) Determination

III. APPLICATION OF DISLOCATION THEORY TO MICROSTRAIN

It is an accepted fact that plastic flow in crystalline solids has its origin in the motion of dislocations. The behavior of a dislocation under the application of a stress to give plastic flow is illustrated in Figures 10 and 11. Figure 10 depicts a dislocation line segment with both screw and edge components. When a shear stress is applied, this segment expands as shown, producing an element of shear with an offset of $\vec{b}$. Figure 11 illustrates a slightly more complex configuration consisting of a dislocation line segment pinned internally at both ends. The application of a stress causes the loop to bow out as shown in parts (a) through (h) of Figure 11, resulting again in an element of slip. In this case, however, the original segment is regenerated and the process can be repeated. This is in essence the classic Frank-Read[18] source mechanism for dislocation multiplication.

The stress σ required to operate the dislocation source is in each case given by an expression, based on the line tension approximation, of the form

$$\sigma = Gb/\ell \tag{3}$$

where G is the shear modulus, b the Burgers vector, and ℓ the source length. The shear strain γ produced by the motion of a dislocation is given by the expression

$$\gamma = Nb\ell \tag{4}$$

where N is the density of moving dislocations in lines/cm^2, and ℓ is the displacement per unit length of dislocation. This can be demonstrated by considering a segment dx of dislocation loop displaced an increment ds as shown in Figure 12. The strain is given by $d\gamma = \vec{b}\ ds\ dx$ per unit area, and

$$\gamma_{total} = N\vec{b} \int_{s=0}^{s=\ell} \int_{x=0}^{x=l} ds\ dx = N\vec{b}\ell \text{/unit area}$$

With these expressions, the plastic strains associated with applied stress can be calculated semiquantitatively. Table 3 gives G, b, and σ for

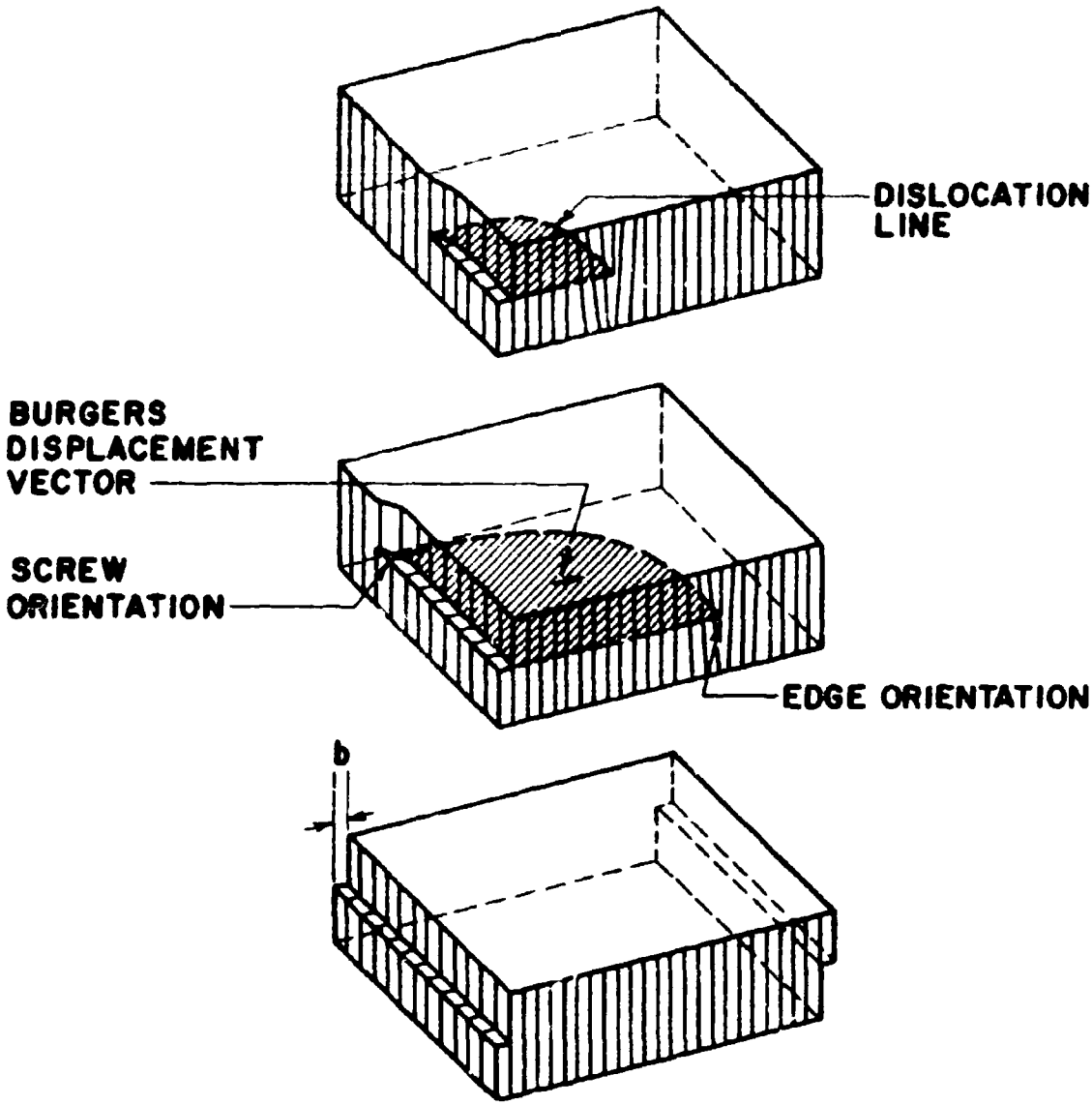

Figure 10. A Dislocation Line Segment with Screw and Edge Components

several engineering materials of interest, with the applied stress σ nominally chosen as 25 percent of the yield stress σ_y of the particular material. For purposes of calculation, initial dislocation densities of 10^4, 10^6, and 10^8 lines/cm^2 have been assumed. The dislocation loop lengths can be estimated from Eq. (3), and the strains can be calculated by substituting the appropriate values into Eq. (4), if it is also assumed that the average displacement per unit dislocation length is approximated by the dislocation loop length ℓ. The results of these calculations are given in Table 4.

Although the calculated strain values are based on some simplifying assumptions, they nevertheless agree reasonably well with experimental values, as can be seen from Table 5 in which the calculated and observed strains for the selected engineering materials are compared. Well-annealed copper exhibits a strain of 1×10^{-6} in./in. at a stress of 1000 psi, which corresponds to a predicted value 4×10^{-6} in./in. for a dislocation density of 10^6 lines/cm^2. The agreement for annealed "A"-nickel is especially meaningful since the dislocation density was experimentally determined[19] to be $\sim 2 \times 10^6$ lines/cm^2. TD-nickel exhibits a strain of $\sim 1.5 \times 10^{-5}$ in./in. at 15,000 psi. This value corresponds to the calculated strain value for TD-nickel with a dislocation density of $\sim 10^8$ lines/cm^2, a reasonable dislocation density for a dispersion-hardened material. A well-annealed sample of 1018 steel exhibits a strain of 6×10^{-6} in./in. at 11,000 psi. This value corresponds to the predicted strain value for low carbon steel having a dislocation density of $\sim 10^7$ lines/cm^2, which is a realistic density for annealed low carbon steel.

As these calculations and approximations indicate, a rather simplified theoretical approach can be used to predict the microstrain behavior to be expected from typical engineering materials.

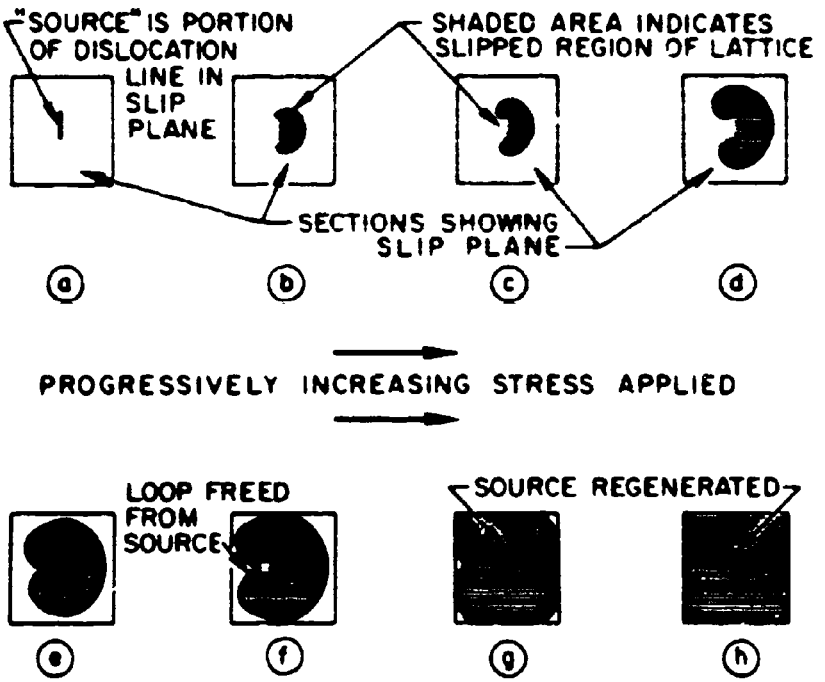

Figure 11. A Dislocation Line Segment Pinned Internally at Both Ends

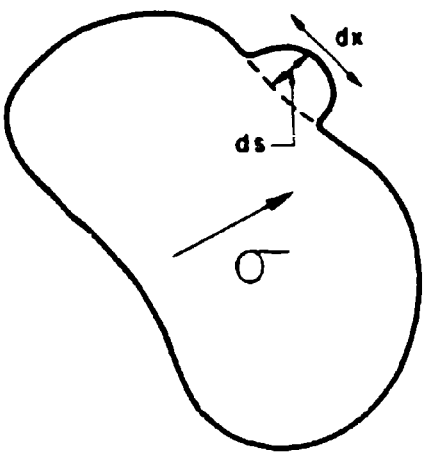

$$\gamma = N\bar{b} \int_{s=0}^{s=\ell} \int_{x=0}^{x=l} ds\, dx = Nb\ell$$

Figure 12. Incremental Displacement of Dislocation Loop Segment

Table 3. Stress, Shear Modulus, and Burgers Vector Values for Selected Engineering Materials

Materials	σ_y, psi	σ, psi	$G \times 10^{-6}$, psi	$b \times 10^{8}$, cm
Low Carbon Steel (SAE 1020)	45,000	11,000	11	2.48
High Carbon Steel	140,000	35,000	11	2.48
Aluminum	5,000	1,250	4	2.86
Duralumin	18,000	4,500	4	2.86
2024-T36 Al	52,000	13,000	4	2.86
Copper	4,000	1,000	6	2.55
Be-Copper	200,000	50,000	7	2.55
"A"-Nickel	10-30,000	2,500-7,500	11	2.49
TD-Nickel	~65,000	15,000	11	2.49

Table 4. Calculated Shear Strains for Selected Engineering Materials

Material	ℓ, cm	γ, in./in.		
		N, lines/cm^2		
		10^4	10^6	10^8
Low Carbon Steel	2.5×10^{-5}	6.2×10^{-9}	6.2×10^{-7}	6.2×10^{-5}
High Carbon Steel	7.8×10^{-6}	1.93×10^{-9}	1.93×10^{-7}	1.93×10^{-5}
Aluminum	9.15×10^{-5}	2.6×10^{-8}	2.6×10^{-6}	2.6×10^{-4}
Duralumin	2.54×10^{-5}	7.26×10^{-9}	7.26×10^{-7}	7.26×10^{-5}
2024-T36 Al	8.8×10^{-5}	2.52×10^{-9}	2.52×10^{-7}	2.52×10^{-5}
Copper	1.53×10^{-4}	3.9×10^{-8}	3.9×10^{-6}	3.9×10^{-4}
Be-Copper	3.56×10^{-6}	9.08×10^{-10}	9.08×10^{-8}	9.08×10^{-6}
"A"-Nickel	1.1×10^{-4}	2.74×10^{-8}	2.74×10^{-6}	2.74×10^{-4}
	3.6×10^{-5}	8.97×10^{-9}	8.97×10^{-7}	8.97×10^{-5}
TD-Nickel	1.8×10^{-5}	4.6×10^{-9}	4.6×10^{-7}	4.6×10^{-5}

Table 5. Comparison of Calculated and Experimental Microstrains

Material	Stress, psi	Strain, in./in.	
		Calculated	Experimental
Copper	1,000	4×10^{-6}	$1\text{-}2 \times 10^{-6}$
"A"-Nickel	2500-7500	$1.5\text{-}5 \times 10^{-6}$	--
"A"-Nickel	2,500	--	$1\text{-}4 \times 10^{-6}$
Niobium	5,000	1×10^{-6}	1×10^{-6} Quenched None Unquenched
TD-Nickel	15,000	4.6×10^{-5}	1.5×10^{-5}
2024-T36 Al	13,000	2×10^{-6}	--
2024-T351 Al	30,000	--	1×10^{-6}
SAE 1020 Steel	11,000	6.2×10^{-6}	--
SAE 1018 Steel	11,000	--	6×10^{-6}
High Carbon Steel	35,000	2×10^{-6}	--
0.8 C Tool Steel	52,000	--	1×10^{-6}

IV. CONCLUSION

Efforts to improve the micro-mechanical properties of materials must, in general, take the same directions as have efforts to improve the engineering mechanical properties of interest. Any approach that will immobilize dislocations or restrict the free path over which they might move will increase the P. E. L. In general, materials with highly directional bonding, i. e., covalent solids and solids with a high elastic modulus, show little or no microstrain. However, this condition is not sufficient to ensure minimal microstrain, as evidenced by beryllium metal, which has a Young's modulus of 42. 5 million psi and exhibits a P. E. L. of 2500 psi. [12]

Kossowsky and Brown[8] have observed that quenched and tempered carbon steels of 0. 95 and 0. 48 percent C show no microstrain prior to their upper yield point indicating the importance of dislocation pinning by precipitates. In this case, the Young's modulus and shear modulus are little affected by compositional changes from the values for low carbon and high carbon steels discussed earlier.

Experimentally, it has also been observed that many materials exhibit radically reduced micro-mechanical strength in a flexural or bending type test when the stress is reversed following a determination of the microstress-strain curve in one direction. This behavior has been termed the micro-Bauschinger[20] effect because of its similarity to the classic Bauschinger effect, and, as shown in Figure 13, this experimental result emphasizes the rather significant influence that residual stress can exert on micro-properties. Such a characteristic, which might easily develop as a result of fabrication and forming practices, would result in most undesirable properties with respect to microcreep resistance, to thermal stresses imposed by even small ambient temperature cycling, and to stresses generated during acceleration and/or centrifugal loading conditions.

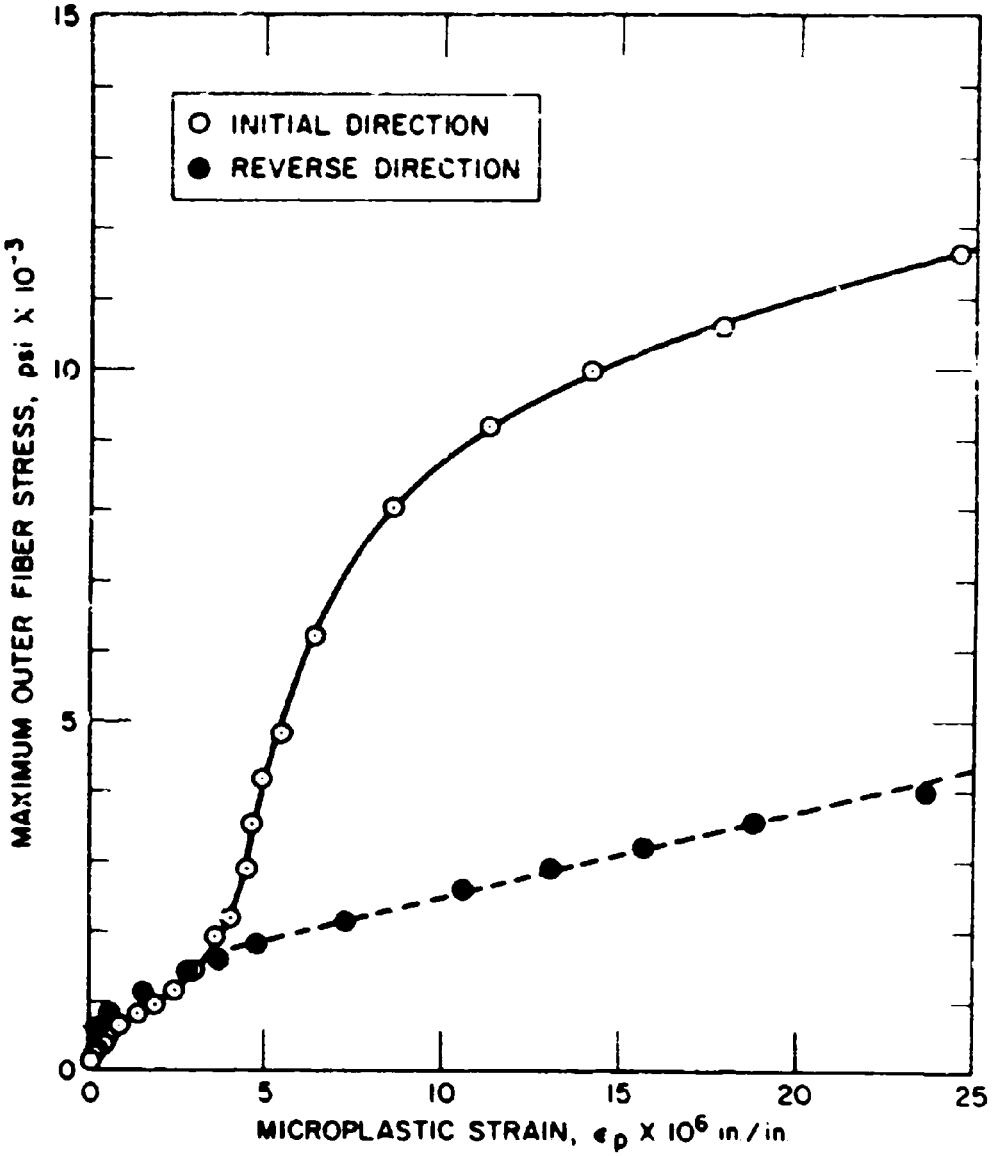

Figure 13. The Micro-Bauschinger Effect

In summary, it must be emphasized that there are two basic reasons for studying microplasticity in the laboratory today. First, as has been emphasized in this review, is the need to specify completely and precisely the mechanical behavior of materials to enable competent selection and profitable application of materials in guidance and control systems. Second is the purely scientific reason for furthering understanding of the basic role of structural imperfections in determining the mechanical properties of solids.

REFERENCES

1. O. Haase and E. Schmid, Z. Physik 33, 413 (1925).

2 D. S. Wood and D. S. Clark, Am. Soc. Testing Mater. Proc. 49, 717 (1949).

3. T. Vreeland, Jr., D. S. Wood, and D. S. Clark, Trans. Am. Soc. Metals 45, 620 (1953).

4. J. A. Hendrickson, D. S. Wood, and D. S. Clark, Acta Met. 4(6), 593 (1956).

5. J. Roberts and N. Brown, Trans. AIME 218, 454 (1960).

6. N. Brown and K. F. Lukens, Acta Met. 9, 106 (1961).

7. J. M. Roberts and N. Brown, Acta Met. 10, 1101 (1962).

8. R. Kossowsky and N. Brown, "Microstrain Study of Dispersion-Hardening in Plain Carbon Steel," Paper presented at the Fall Meeting of the Metallurgical Society, October 30, 1962.

9. G. Harter, Inertial Guidance, ed. G. R. Pitman, Jr., John Wiley and Sons, Inc., New York (1962), pp. 294-310.

10. G. R. Pitman, Jr., Inertial Guidance, ed. G. R. Pitman, Jr., John Wiley and Sons, Inc., New York (1962), p. 429.

11. J. J. Jarosh, Inertial Guidance, ed. G. R. Pitman, Jr., John Wiley and Sons, Inc., New York (1962), p. 113.

12. W. Bonfield and C. H. Li, Acta Met. 12, 577 (1964).

13. R. D. Carnahan and J. E. White, Trans. AIME 230, 249 (1964).

14. R. D. Carnahan and J. O. Brittain, J. Appl. Phys. 34(10), 3095-3104 (1963).

15. R. D. Carnahan, Ph. D. Dissertation, Northwestern University, Evanston, Ill. (1962).

16. J. J. Gilman and W. G. Johnston, J. Appl. Phys. 29(6), 877-88 (1958).

17. F. W. Young, Jr., J. Appl. Phys. 32, 1815 (1961).

18. W. T. Read, Jr., Dislocations in Crystals, McGraw-Hill Book Co., Inc., New York (1953).

19. R. D. Carnahan and J. E. White, "The Microplastic Behavior of Polycrystalline Nickel," Phil. Mag. (1964). In Press.

20. R. D. Carnahan and J. E. White, The Microplastic Behavior of Polycrystalline Nickel, TDR-269(4240-10)-5, Aerospace Corporation, El Segundo, Calif. (6 January 1964).